Externally Dispersed Interferometry for Planetary Studies

David J. Erskine[a], Jerry Edelstein[b], Daniel Harbeck[b] and James Lloyd[c]

[a]Lawrence Livermore Nat. Lab., 7000 East Ave, Livermore, CA 94550
[b]Space Sciences Lab. at Univ. of Calif., Berkeley, CA 94720-7450
[c]Astronomy Dept., Cornell University, Ithaca, NY 14853

ABSTRACT

We describe a plan to study the radial velocity of low mass stars and brown dwarfs using a combination of interferometry and multichannel dispersive spectroscopy, Externally Dispersed Interferometry (EDI). The EDI technology allows implementation of precision velocimetry and spectroscopy on existing moderate-resolution echelle or linear grating spectrograph over their full and simultaneous bandwidth. We intend to add EDI to the new Cornell TripleSpec infrared simultaneous JHK-band spectrograph at the Palomar Observatory 200" telescope for a science-demonstration program that will allow a unique Doppler-search for planets orbiting low mass faint M, L and T type stars. The throughput advantage of EDI with a moderate resolution spectrograph is critical to achieving the requisite sensitivity for the low luminosity late L and T dwarfs.

Keywords: Doppler planet search, radial velocity, externally dispersed interferometer, EDI, interferometry, high resolution spectroscopy

1. INTRODUCTION

The flourishing detection of exoplanets is providing us for the first time in history with data to test our theories of the possible worlds around other stars. Everything we have learned about exoplanets - Jupiters in 0.1 AU orbits high eccentricities, planets in resonances - is unexpected. The detection of extrasolar planets by the radial velocity (RV or Doppler) method is central to this quest. The RV measurement is extremely challenging. Typical planetary shifts are 1000 times smaller than the stellar line widths, requiring extremely stable and well-calibrated instrument characteristics in order to separate the shift from environmentally induced instrumental drift. Since the detectable planet mass is directly proportional to the velocity precision, high velocity precision is needed to detect planets of small mass and to detect long period planets.

The conventional RV measurement approach uses high-resolution dispersive spectrographs ($\lambda/\delta\lambda$ = R$\sim$50-100 k) to obtain the velocity precision required for planet hunting. These instruments are typically large and costly echelles with large optics and paths that must be held to high mechanical tolerances over many-meter distances. These instruments suffer from low throughput and maintaining long-term stability often requires substantial effort such as complex servo systems or huge vacuum tanks.[1–3] Current planet search samples are limited to bright stars in the optical band, thus inhibiting knowledge about the populous low mass stars that are important for discriminating among planet formation theories. In this paper we outline a Doppler survey for planets orbiting low mass stars and brown dwarfs using a combination of interferometry and multichannel dispersive spectroscopy, Externally Dispersed Interferometry (EDI), which dramatically improves the velocity resolution of moderate resolution, high throughput spectrographs.

1.1. Cool Star Radial Velocity Survey

Low mass stars and brown dwarfs dominate the stellar population in both number and total mass. As the mass of the primary decreases, the radial velocity signature increases: $v = 28ms^{-1}\ \frac{(m_p/M_J)\sin(i)}{(P/yr)^{1/3}(M/M_\odot)^{2/3}}\ \sim \frac{m_p}{M^{2/3}}$ where

Further information: http://www.spectralfringe.org/EDI
D.E.: erskine1@llnl.gov, Tele.: 925-422-9545
J.E.: jerrye@ssl.berkeley.edu, Tele.: 510-642-0599
D.H.: harbeck@ssl.berkeley.edu, Tele.: 510-643-0696
J.L.: jpl@astro.cornell.edu, Tele.: 607-255-4083

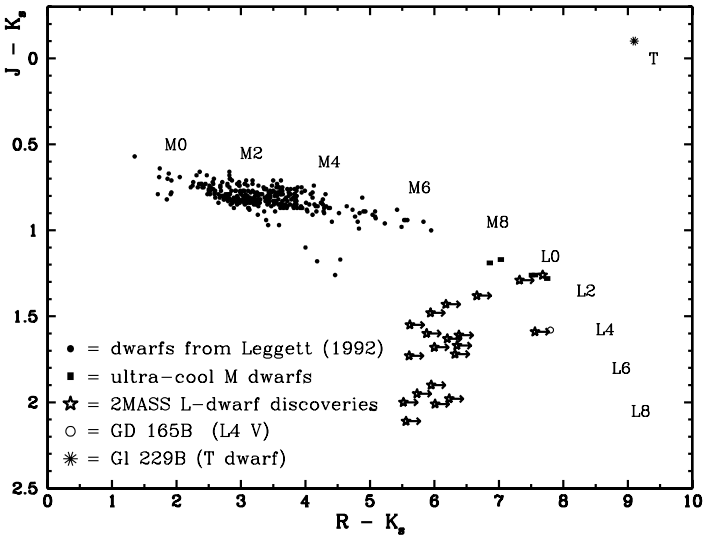

Figure 1. colors of M, L, and T stars (from Ref. 4). The rapidly cooling atmospheres of low mass stars results in extremely red colors. Near Infrared measurements of cool stars and brown dwarfs are advantageous due to the large flux relative to other bands.

m_p is the mass of the planet, M is the mass of the star, M_J is a Jupiter mass and $M_\odot$ is a solar mass. Therefore low mass stars provide a favorable signal for the detection of low mass planets.

Of the plethora of planets detected, nearly all of their host star masses lie in the range 0.7 - 1.4 $M_\odot$. Stars more massive than 1.4 $M_\odot$ are simply not amenable to radial velocity studies due to the featureless spectra from their hot atmospheres. Stars less massive than 0.7 $M_\odot$ cool rapidly and become increasingly faint in the green-visible, the widely-used iodine absorption-line reference cell's bandpass. Past and present radial velocity surveys are limited to the earliest M stars, become rapidly incomplete beyond M2-M3, and are completely incapable of extending into the brown dwarf spectral classes. Indeed, the problem of studying cool star planets has been flagged as a key science question for the next generation of Gemini telescope instrumentation.

We plan to undertake a novel near infrared radial velocity study of the lowest mass stars and brown dwarfs by implementing EDI for the TripleSpec spectrograph on the Palomar 200". Nearly all the emergent flux from these stars is in the near infrared (NIR) (see Fig. 1). The large simultaneous JHK band wavelength coverage of TripleSpec and the high throughput of this moderate resolution spectrograph are ideal for demonstration of EDI radial velocity studies. The throughput advantage of EDI with this moderate resolution spectrograph is critical to achieving the requisite sensitivity for the low luminosity late L and T dwarfs. This combination will provide, for example, a photon limited Doppler resolution of 3.25 m/s for $m_H = 7$ in a 1-hour exposure as well as full echelle-band spectral observations at an effective resolution of R ∼10,000.

2. EDI PRINCIPLES, PERFORMANCE

The externally dispersed interferometer[5–8] is a general technique that can enhance the performance of any style of grating or prism spectrograph used for Doppler velocimetry or classical spectroscopy. The EDI can increase the Doppler sensitivity and multiply the spectral resolution of an existing spectrograph over the spectrograph's full and simultaneous bandwidth by a factor of several to an order of magnitude while preserving imaging.[9] For example, our prototype observatory and laboratory instruments have demonstrated EDI visible-band velocimetry precision to ∼5 m/s using an R= 20,000 spectrograph, and a factor of six increase[10] in conventional spectrograph resolving power (from R= 25 k to R= 140 k).

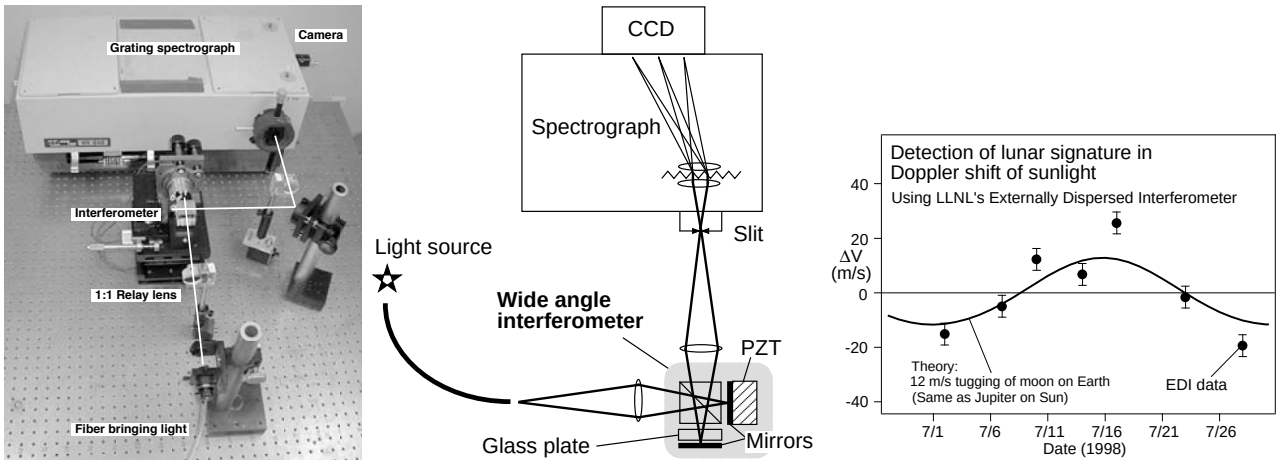

Figure 2. Laboratory EDI spectrograph photo and schema. Light, after traversing an optional calibrating absorption cell, traverses a small, unequal-arm, wide-field Michelson interferometer and is focussed onto the slit of a conventional grating spectrograph. This instrument used a R=20k spectrograph and τ=1 cm delay interferometer to achieve an effective resolution of R$\sim$50 k and was used to detect[5] the 12 m/s Doppler signature in sunlight due to the Moon's gravity on Earth **(Right)**. This is the same size effect as a Jupiter-like planet pulling a $M_\odot$ star. Velocity stability of $\sim$1 m/s and $\sim$4 m/s was measured for short (20 min) and long (4 wk) durations, respectively (Fig. 4). Neither thermal or convection control was used and the optics were off-the shelf components.

2.1. Interferometer and Spectrograph in Series

An externally dispersed interferometer (EDI) is a series combination of a fixed delay interferometer and an external dispersive spectrograph (see Fig. 2-Left). Fringes created by the interferometer are imaged to a spectrograph's slit. These fringes provide a periodic spectral fiducial comb covering the entire bandwidth of the spectrograph. The interferometer transmission comb is sinusoidal in wavenumber ($\nu = 1/\lambda$). This comb is analogous to the fiducial lines of an iodine absorption cell, but with lines of exceedingly uniform spacing, shape, and amplitude over the entire bandwidth. The comb, in multiplication with the input spectrum, heterodynes fine spectral features into a low spatial-frequency moiré pattern (see Fig. 3-Right) that is recorded by the spectrograph detector. This pattern survives the blurring of the spectrograph, whereas the absorption lines themselves may not. The heterodyning is numerically reversed to recover detailed spectral and doppler information otherwise unattainable due to the spectrograph's inherent resolution or detector Nyquist limits.

A Doppler effect shifts the fringe phase of each absorption line in the spectra. In EDI, the moiré fringe phase becomes the primary diagnostic instead of spectral dispersion. Since these shifts are nearly the same over the entire bandwidth, they can be averaged together to produce a strong net signal. These rotate in phase versus the Doppler shift Δv_D as $e^{i2\pi\tau\Delta v_D}$ where τ is the delay in the interferometer arms. A vector data analysis procedure[5] precisely measures the differential moiré pattern phase between the input spectrum and a reference spectrum (absorption cell or emission lamp) that has been simultaneously recorded in the same fringing signal. The phase difference yields the Doppler velocity, independent of moderate changes in τ.

EDI differs from previous heterodyning hybrids[11–13] by using a dispersing element that is external, rather than internal, to the interferometer. Unlike these other methods, EDI's spectral fringe periodicity is nearly uniform in wavenumber, allowing for a larger (unlimited) operating bandwidth. In comparison with a dispersed Fabry-Perot interferometer producing spike-like spectral fiducials,[14,15] EDI's sinusoidal fiducial fringes transmit greater average flux, offer simple Fourier heterodyning reduction schemes, and allow elegant trigonometric recovery of precise spectral information from as few as three phase-stepped data recordings.

EDI's sensitivity greatly exceeds that of the purely interferometric Fourier Transform Spectrograph (FTS) and is comparable to conventional spectrographs because of EDI's large simultaneous bandpass and because throughput losses due to extra interferometer optical elements can often be more than recovered by using EDI's resolution gain that allows for an increase in spectrograph input slit width.

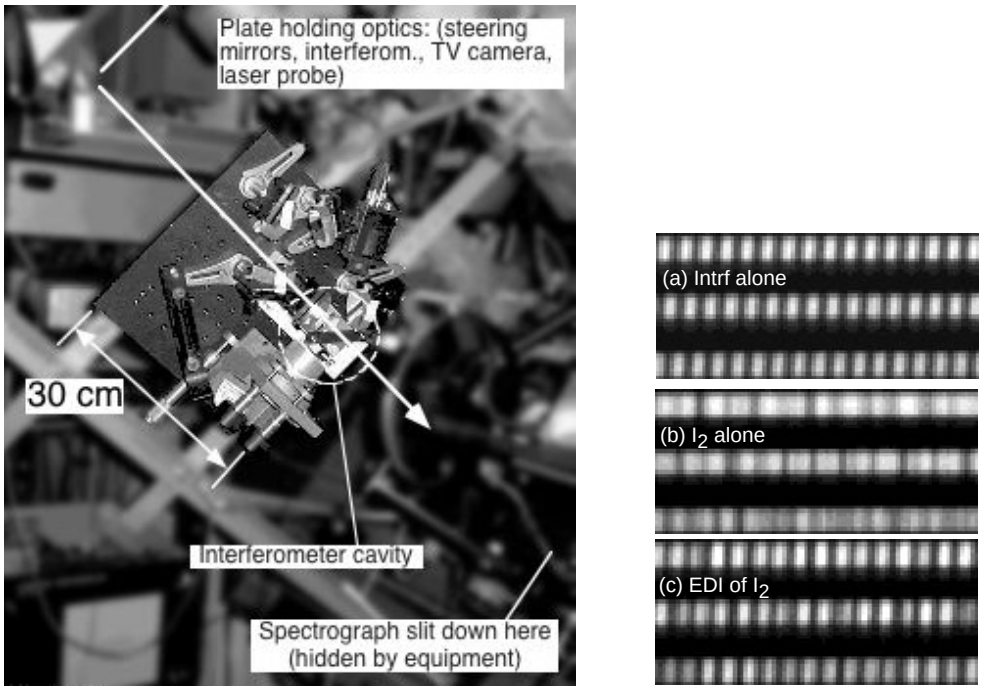

Figure 3. interferometer installed before the slit of the Lick echelle spectrograph. Starlight from the telescope passes through the interferometer, which is mounted on a 30 cm square plate. Fringes created at the interferometer are imaged to the spectrograph slit by a lens; the latter two are hidden. A reference iodine cell could be inserted into the beam before the slit. **(Right)** Raw EDI echelle spectrograph data. A sample of 3 echelle orders are shown vertically separated for a quartz continuum lamp source. (a) Interferometer alone. The spectral fringes are dispersed horizontally and appear as a sinusoidal bead-like pattern. (b) Iodine cell alone yields an ordinary absorption spectrum. (c) Iodine with interference– an EDI spectrum– is optically (a)x(b). Moiré patterns are created.

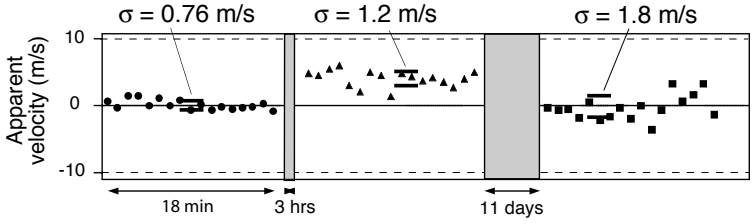

Figure 4. in optical lab. Back-lit bromine absorption cell was a zero velocity reference source. Short term noise <1 m/s over 18 minutes. Zero point drift stability for longer term durations (3 hrs and 11 days) were <4 m/s. Measurements taken at ambient laboratory conditions with no special environmental control.

2.2. Demonstrations & Principles

We illustrate EDI principles and performance through description of our observatory and laboratory EDI prototype demonstrations. Our work has been used for radial velocity measurements of starlight[7] and sunlight[5] and for broadband high-resolution absorption spectroscopy.[9,16] This work included extensive development of the essential theory and data-reduction algorithms. For example, our EDI measurements have detected the 12 m/s amplitude of the Moon tugging the earth (see Fig. 2-Right) over a 1-month duration with an 8 m/s scatter attributed to telescope pointing instabilities.[5] Other workers have adopted the EDI method from our laboratories and demonstrated a Doppler planet detection.[17]

An example of the EDI fringing signal and its combination with the spectral signal is shown in Fig. 3-Right.

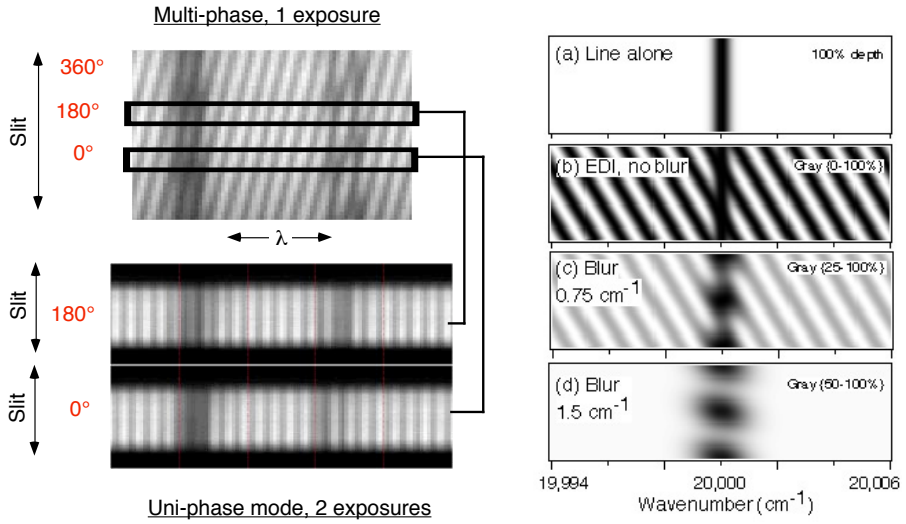

Figure 5. (Left) Multi-phase (a) and uni-phase (b) recording. In multi-phase all phases are recorded in a single exposure– phase varies (slanted) along slit. In uni-phase, phase is constant over the slit, allowing zero slit-height beams for imaging and echelle spectroscopy. **(Right)** The EDI moiré pattern persists in the presence of spectrograph blurring that far exceeds the intrinsic width of the absorption line observed. A simulated Gaussian absorption line (a) is multiplied by (slanted) EDI fringes in the spectral or horizontal axis (b). The varying fringing phase beats with the spectral line to form a moiré that persists when the spectral resolution is blurred (c) to the point that the EDI fringes themselves can no longer be resolved (d).

Data were acquired using the full bandwidth of 4000-8000 Å of the Lick Observatory's Hamilton 2-d echelle spectrograph[2] and a prototype EDI interferometer (see Fig. 3-Left) using a wide angle Michelson design.[18] The 30 cm sized interferometer requires only $\lambda/3$ path length stability during an exposure, unlike the extreme stability required for white-light fringe interferometers. The Lick apparatus was designed to demonstrate basic EDI performance and was not optimized for sensitivity– we discarded one interferometer arm output, a 50% loss. (Our planned instrument uses both interferometer outputs.)

2.3. Uniform vs Multi-phase Recording

In order to reject systematic noise, EDI data are acquired using a method where the phase of the interferometer fringe ($\phi = 2\pi\delta\tau/\lambda$), set by the path delay τ, is spatially or temporally varied. We arrange to collect at least three (and more conveniently four) phase steps either simultaneously or in sequence. The phased data are combined using an algorithm that constructively adds the fringing science-signal phases, and destructively combines the fixed-pattern noise terms. The phase combination algorithm is an additive process that recovers the entire photon signal– no photon noise penalty is incurred. This is in contrast with subtraction algorithms that can cause large errors by seeking a small residual from the difference of two large signals. Phased data preserves the photon signal but does cause some detector read noise penalty. When working in the photon limited domain or extracting extremely precise velocity resolution, the gain in rejection of common mode and systematic errors that plague conventional spectroscopy is dramatic and beneficial.[5]

Phased data can be taken in two modes with the phase either uniform (uni-phase) or varying (multi-phase) along the slit length (Fig. 5-Left). In the uni-phase fringe mode, the interferometer mirrors are parallel, ϕ is made constant over the slit and a minimum of three phase-stepped exposures are acquired. In the multi-phase fringe mode, an interferometer mirror is tilted so that ϕ varies spatially across the slit's length and the full ϕ range is sampled in at least three bins within a single exposure. The uni-phase mode (Fig. 5-Left b) can be used with zero slit-length, which permits EDI application to 1-d imaging or echelle spectroscopy where the cross-dispersion dimension must be minimized to retain angular or order information.

Rejection of the errors caused specifically by detector pixel non-uniformities (e.g. distortion, gain) is the most effective when the phase-stepped exposures are recorded using the identical pixels. Thus while not required, multi-phase recording is best temporally phase-stepped to record the phase steps on the same pixels. Dividing an exposure for phase-acquisition causes a detector read noise penalty. Both phase modes require at least three reads to acquire phase-steps on identical pixels. For the multi-phase mode, the target's light must be spread along the slit so that the phases can be simultaneously recorded, causing an additional factor of $\sqrt{3}$ read noise. For background limited observations, the signal to noise is degraded by 1.7× for uni-phase and 3× for multiphase. The optimum data acquisition strategy depends on signal strength, sensor noise, and observing overhead factors. The read-noise penalty does not impact our Doppler measurements because they will be in the photon-limited regime, using either the uni- or multi-phase mode.

2.4. EDI Theory

The conventional (purely dispersive spectroscopy) detected signal versus wavenumber, $B_{ord}(\nu)$, is the convolution of the intrinsic input spectrum, $S_0(\nu)$, and the spectroscope line spread function $LSF(\nu)$,

$$B_{ord}(\nu) = S_0(\nu) \otimes LSF(\nu) \ . \tag{1}$$

The convolution of Eq. 1 is conveniently expressed in Fourier-space as a product,

$$b_{ord}(\rho) = s_0(\rho) lsf(\rho), \tag{2}$$

where lower case symbols are the transforms, and ρ is the spatial frequency along the dispersion axis in features per cm^{-1}. The *lsf*(ρ) is thus the transfer function of the impulse response $LSF(\nu)$. The normalized interferometer transmission $T'(\nu)$ is a sinusoidal spectral comb,

$$T'(\nu) = 1 + \gamma \cos(2\pi\tau\nu + \phi) \ , \tag{3}$$

where γ is the interferometer visibility, assumed unity for now, and τ and ν in units cm and cm^{-1}, respectively. Raw fringing spectra B_ϕ are recorded at multiple phase values ϕ differing by $\sim 90°$, designated B_0, B_{90}, etc. The passage of light through the interferometer multiplies the spectral comb $T'(\nu)$ with the spectrum prior to blurring by the external spectrograph. Hence the EDI detected signal is

$$B_\phi(\nu) = [S_0(\nu)\ T'(\nu)] \otimes LSF(\nu) \ . \tag{4}$$

This is re-expressed as a sum of the ordinary spectrum plus two complex counter-rotating fringing components:

$$B_\phi(\nu) = B_{ord}(\nu) + 1/2[S_0(\nu)e^{i\phi}e^{i2\pi\tau\nu} + S_0(\nu)e^{-i\phi}e^{-i2\pi\tau\nu}] \otimes LSF(\nu). \tag{5}$$

High-resolution information is recovered by isolating a fringing component and reversing the heterodyning. The scalar spectrum is converted to a complex vector spectrum called a "whirl", $\mathbf{W}(\nu)$, by using a linear combination of the phased exposures B_ϕ with the phases numerically synchronized to each exposure's phase-step value. The whirl for a four phase recording every 90° is

$$\mathbf{W}(\nu) = 1/2(B_0 e^{i0^\circ} + B_{90} e^{i90^\circ} + ...), \tag{6}$$

or

$$\mathbf{W}(\nu) = 1/4[(B_0 - B_{180}) + i(B_{90} - B_{270})]. \tag{7}$$

The whirl is then:

$$\mathbf{W}(\nu) = 1/2[S_0(\nu)e^{i2\pi\tau\nu}] \otimes LSF(\nu) \ . \tag{8}$$

and the Fourier transform of the whirl is

$$\mathbf{w}(\rho) = (1/2)\gamma\ s_0(\rho + \tau)\ lsf(\rho) \tag{9}$$

where we include the interferometer visibility (γ) previously taken as unity. This important equation describes the EDI formation of moiré fringes, a heterodyning effect expressed in the $s_0(\rho + \tau)$ argument. Fine spectral details having high feature density ρ are heterodyned (shifted by τ) to measurable low density, ρ features prior to any blurring by the spectrograph's line spread function. The ordinary spectrum is determined by summing the phase-stepped data so that fringing terms cancel,

$$B_{ord}(\nu) = 1/4(B_0 + B_{180} + B_{90} + B_{270}) \ . \tag{10}$$

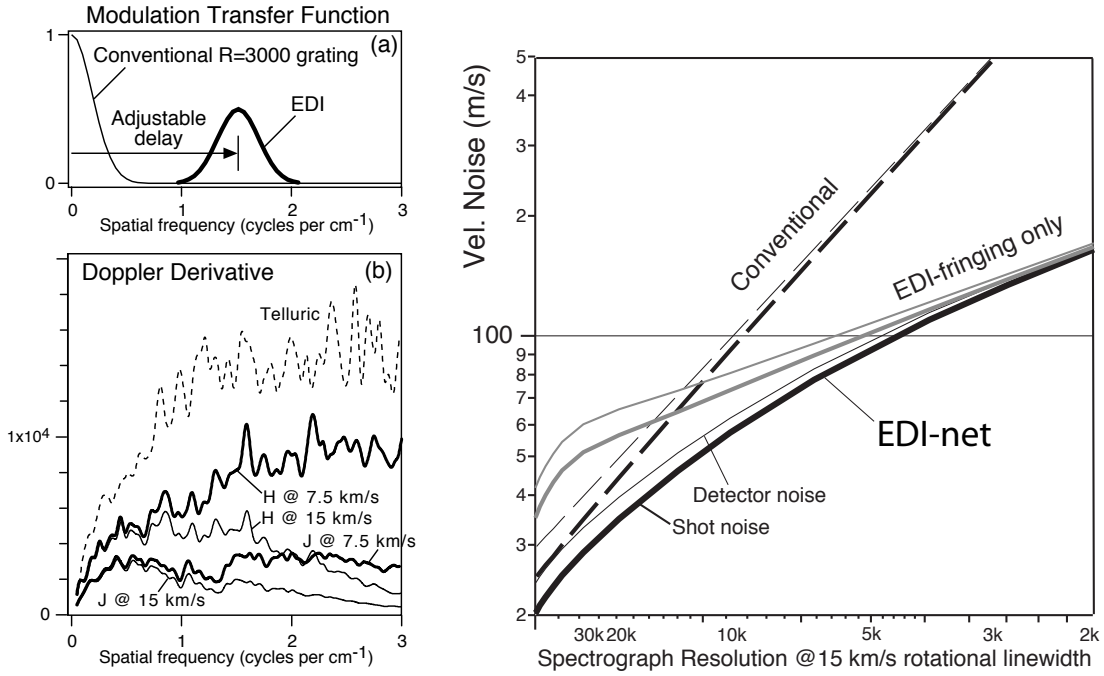

Figure 6. (Left) (a) Spectrometer Frequency Response (modulation transfer function) is the instrument's ability to measure a given spatial frequency in the dispersion direction. Thin curve is conventional grating and R=3000 at 1.7 microns. Bold curve is EDI heterodyning response, adjustable by delay (τ). (b) Doppler information content vs spatial frequency calculated for the J & H bands of a sunspot (surrogate M dwarf spectra) and Telluric spectrum. This is the FFT of the spectral derivative weighted by wavenumber. Stellar rotational velocities v sin(i)=7.5 km/s (bold) and 15 km/s (thin) effects. EDI Doppler measurement is optimized by setting delay at Doppler information maximum. **(Right)** Doppler velocity noise calculated for a single Gaussian line of 0.25 cm^{-1}line width and 50% absorption depth at ν=5000 cm^{-1} receiving 0.5x10^6 photons/cm^{-1} in the continuum, for conventional and EDI Doppler measurements. The EDI-net curve includes both fringing and nonfringing components. EDI especially improves velocity noise for lower resolution spectrographs.

2.5. EDI Doppler Response

For a nonrelativistic velocity V, the wavenumber scales as $\nu \rightarrow (1 + V/c)\,\nu$, so that over a limited bandwidth there appears to be a shift $\Delta\nu_D = (\Delta V/c)\,\nu$. The EDI Doppler measurement uses the change in moiré phase. The moiré pattern is described by the whirl: $W(\nu) = \frac{1}{2}\left[e^{i2\pi\tau\nu} S_o(\nu)\right] \otimes LSF(\nu)$. A Doppler shift causes the whirl to rotate: $W_1(\nu) = W_0(\nu)\, e^{i2\pi\tau\Delta\nu}$ by an angle $\theta = \tau\Delta\nu_d$. Changing $\tau\Delta v_D$ by unity corresponds to a whirl revolution and the velocity per fringe proportionality (VPF) is VPF= $(\lambda/\tau)c$. The VPF for $\lambda = 1.66\,\mu$m and $\tau = 2$ cm, is $\sim 25,000$ m s^{-1} per fringe. We make a simultaneous measurement of both the stellar and reference (cell) spectra, and thus the same value of τ applies to each. Since the Doppler velocity is a difference between those two components, EDI is robust against instrument instabilities causing small drifts in τ.

2.6. Doppler Signal Information

The quality of Doppler information within a bandpass depends on the number of spectral lines, their strength and width. The signal for a Doppler shift is proportional to the typical slope of spectral features, that is the characteristic derivative of the spectrum $\delta S/\delta\nu$, which in ρ-space is $\rho s_0(\rho)$. Furthermore, it should be weighted by the wavenumber to be $\rho\; s(\rho)\,\nu$, since the absolute Doppler shift scales with wavenumber.

The best sampling frequencies for Doppler measurements consequently depend on the specific stellar spectra under study. Due to the lack of available high resolution NIR spectra of cool stars, we use as a proxy the J and H bands from the NSO sunspot spectra. The sunspot corresponds to ∼5000 K, similar to K0 at 5300, and is cool enough to allow some molecule formation. For our cool star surrogate, the important Doppler spatial frequencies are shown in Fig. 6-Left(b) for stellar rotational velocities v sin(i) = 7.5 and 15 km/s. Rotation will blur the stellar lines and limit attainable high spatial frequencies. We find that the H-band has a more Doppler information than the J-band and that for v sin(i) = 7.5 km/s and 15 km/s rotational velocities, most of the information occurs at spectral feature frequencies of ∼1- 2 cm^{-1}.

The advantage of EDI RV measurements now becomes evident. The EDI peak response to spatial frequencies is set by the interferometer delay (τ). Fig. 6-Left(a) illustrates how the EDI ρ response, which is the scaled conventional spectrograph response shifted by τ, can be selected to sample the maximum Doppler signal region and measure high spatial frequencies far beyond the spectrograph's resolution limit. The conventional spectrograph alone samples an inferior Doppler signal because it responds only to low frequency features centered at ρ=0 where the Doppler information content is small.

An important property of EDI is that its spectral response has an extremely symmetric and stable sinusoidal basis due to the interferometer. The most stable region of the grating response $lsf(\rho)$ is shifted from low to high spatial frequencies, where the desired science information resides. Therefore, unlike a classical spectrograph, the EDI spectral performance is very tolerant of spectrograph and telescope quality and change. Fig. 5-Right shows the heterodyne feature's remarkable persistence in the presence of spectrograph blur.

2.7. Doppler Signal Sensitivity

Table 1. The Relative Sensitivity of EDI vs conventional spectroscopy (R=3,000) for a surrogate cool star spectra (sun spot) at different stellar rotational rates v sin(i). The RMS spectral slope (Q_{edi}) for an EDI measurement using an optimized delay far exceeds the conventionally measured value (Q_{conv}). The net EDI slope (Q_{c+e}) is obtained by the combination of conventional and EDI signals. The net EDI Sensitivity exceeds that of the conventional spectrograph by up to an order of magnitude. Telluric lines will not degrade the spectral Doppler signal because the telluric Q far exceeds the stellar Q.

Spectrum	Band	Rotation km/s	Delay cm	Q_{EDI}	Q_{conv}	Q_{c+e}	Sensitivity c+e/conv
Stellar	H	7.5	2.2	600	180	625	12.1
Stellar	H	15	1.3	300	180	350	3.8
Stellar	H	30	0.5	200	180	270	2.3
Stellar	J	7.5	2.2	160	100	190	3.6
Telluric	H or J	0	2.2	1200	200	1216	37.0

The radial velocity measurement noise is a function of the characteristic spectral derivative and the number of photons recorded. The photon limited velocity noise (δV) in a RV measurement is given by[19]

$$\delta V = \frac{c}{Q}\frac{1}{\sqrt{N}} \tag{11}$$

where N is the total number of detected photons summed over the bandwidth, Q is a dimensionless RMS average of the spectrum's derivative. Therefore, Q is high and the noise is low when the spectral lines are numerous and narrow. Q can be used to express which spatial frequencies in the spectrum are the strongest carriers of Doppler information (see Fig. 6-Left b). For a conventional spectrograph,

$$Q^2_{conv} = \frac{\langle(\nu^2/S)(\partial S/\partial\nu)^2\rangle}{\langle S\rangle} \tag{12}$$

Table 2. EDI Doppler Velocity Noise calculated ($\delta V = \frac{c}{Q}\frac{1}{\sqrt{N}}$) for a 1 hour observation of H=10 and H=14 stars with v sin(i) = 7.5 km/s, for the planned EDI-TripleSpec on the Palomar 200 telescope with a 20% end to end efficiency. F_0 is the H=0 photon flux in the given band. N_{10} is the number of photons acquired for an H=10 star in 1 hour. The K band response has not yet been calculated and should contribute to further reduce the velocity noise. The H=10 star can be measured at the desired δV = 100 m/s in 1 minute.

Band	F_0	N_{10} (1hr)	Q_{Rot}	$\delta V_{m=10}$	$\delta V_{m=14}$
J	2.4 10^{10}	8.6 10^9	190	17 m/s	107 m/s
H	1.5 10^9	5.4 10^8	625	21 m/s	132 m/s
J+H				13 m/s	82 m/s
K	1.5 10^9	5.4 10^8	–	–	–

where in this case S is $S_{star} \otimes LSF$, the stellar spectrum after it has been blurred by the spectrograph line spread function. For the EDI,

$$Q_{edi}^2 = \frac{\langle(\nu^2/S)|\partial\mathbf{W}/\partial\nu|^2\rangle}{\langle S\rangle} \tag{13}$$

where the EDI response **W** senses the input spectrum before it is blurred by the spectrograph (see Eq. 9) so that a much larger derivative and sensitivity than the conventional case can be obtained.

Because the EDI process recovers both a conventional and a fringing spectrum, further advantage can be obtained by combining both signals to form a net EDI signal (see Fig. 6-Right). The two spectral components are determined from different spatial frequencies on the detector and are statistically independent with uncorrelated errors. The net EDI signal Q_{net} is then formed from the component Q quadrature sum. Forming the net EDI signal can provide a useful gain when Doppler information is limited by large stellar rotational velocities or by the spectrum itself, which limits high spatial frequency content.

We calculate the sensitivity and velocity noise for EDI and conventional spectroscopy for our surrogate cool star spectrum (sunspot) in the J and H bands. The umbral input spectrum was first blurred to simulate the stellar rotational rate and then filtered according to either the conventional or EDI frequency response. We used a Gaussian R=3,000 spectrograph response with a delay τ matched to the Doppler information, as described above. Our results (see Tab. 1) show that Q_{edi} far exceeds Q_{conv} and that the H band contains more Doppler information that the J band. The EDI Doppler sensitivity (number of photons, N, required to obtain a velocity error, δV, (see Eqn. 11) **is improved by up to an order of magnitude compared that of the conventional spectrograph**.

The absolute sensitivity and spectral noise is shown for the J and H band in Tab. 2 for the planned EDI-TripleSpec spectrograph on the Palomar 200 telescope, with an estimated total throughput of 20%. The velocity noise for the J and H band is similar since the higher J band flux offsets the better H band Doppler information content. By combining the J and H band data for a $m_H = 10$ star, a velocity noise of 100 m/s can be obtained in 1 minute, and for a $m_H = 14$ star, in 1 hour. We expect that the K band can also be used for further sensitivity gain.

A reference cell and the atmosphere also imprints spectral information in the signal and so can effect the velocity noise. Since the H and J band components have large Q they will not significantly degrade the result since the noise adds in quadrature. Our EDI instruments have already demonstrated a <5 m/s RV measurement noise performance in the observatory and in benchtop tests[7] over durations from 11 days to a month, and achieved near photon limited velocity noise, a remarkable result given the prototype instrument quality and absence of environmental controls (see Fig. 4). This is more than sufficient for the planned 3 to 5 day observing periods.

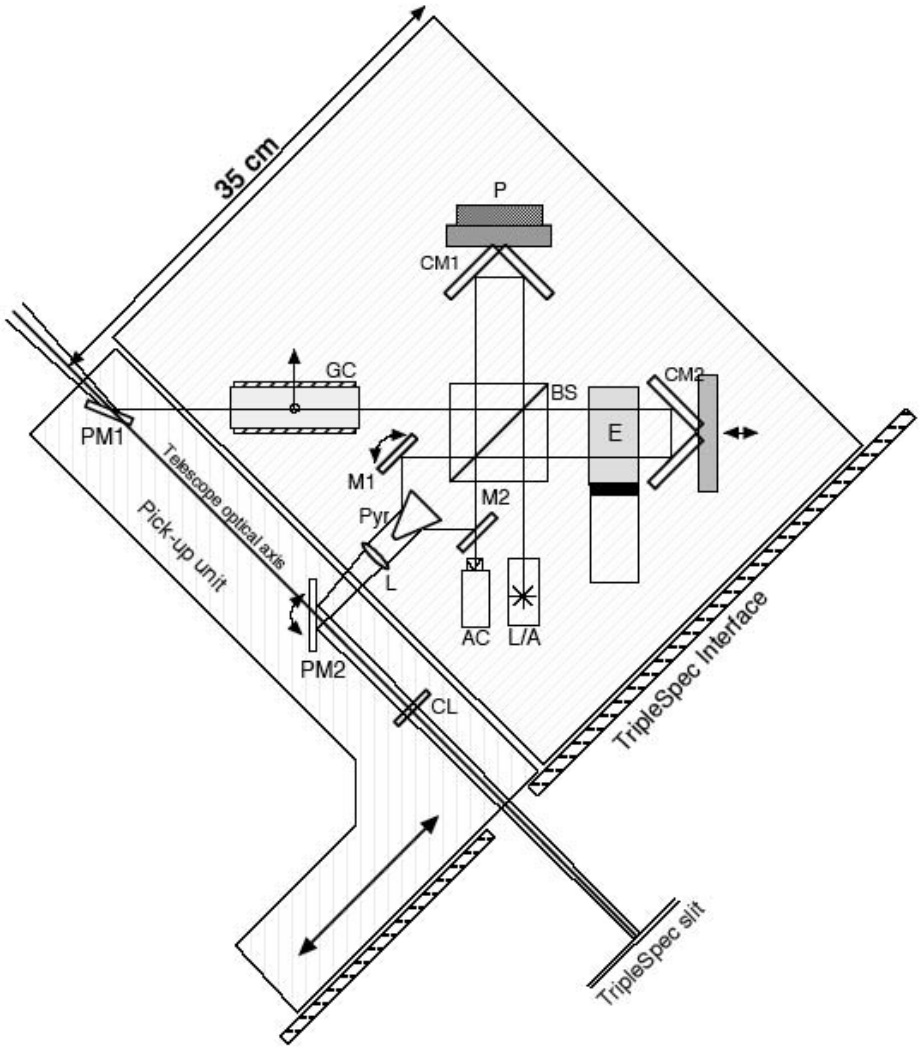

Figure 7. EDI TripleSpec Functional scheme: A movable pick-unit diverts the incoming beam through the EDI interferometer (beamsplitter BS) to focus near the corner mirrors CM_1, CM_2). A gas cell (GC) can be shifted into the beam. The selectable etalon (E) compensates the adjustable unequal-arm path difference. The path difference is stabilized by a piezo mount (P) in a control loop using an out of plane equivalent path reference laser (L/A) and camera (AC). A calibration source (L/A), below the laser, inserts light into the system in-plane. Mirrors M_1, M_2, and a mirrored prism (Pyr) aim the two output beams to adjustable adjacent locations along the TripleSpec slit. The transfer lens L focuses light to the slit width via the alignable return pick-unit mirror PM_2, while the adjustable cylinder lens CL spreads light along the slit for multiphase fringe acquisition. The flux-weighted timer diode/pickoff is not shown.

3. EDI-TRIPLESPEC INSTRUMENT

The TripleSpec-EDI system consists of an interferometer (Fig. 7) mounted to the TripleSpec front plate (in a 35 cm radius volume available to the telescope Cassegrain feed), and a remote control system. The interferometer consists of a fixed main optical unit and pick-up unit that can be moved to intercept the incoming f/16 telescope beam, divert it to the interferometer, and return the light to the beam path for TripleSpec.

The interferometer uses a corner mirror Michelson scheme that allows ready access to both the arms' outputs and to a common-path secondary input for calibration, alignment and stabilization source input. A selectable etalon in one arm creates a nearly angle-independent optical path to allow for a large field of view. Absorption cell selection can be actuated on the input path. Transfer optics reimage the interferometer output to the TripleSpec entrance slit. The complementary output are simultaneously detected by displacing them vertically by 1/2 order. To allow simultaneous multiphase recording, a cylinder lens can be inserted to spread the starlight from each arm in one dimension along the slit length. We expect a net interferometer efficiency of ∼85% based on our plan to use both complementary interferometer outputs and components with high-quality AR and mirror coatings.

Recording fringes over a long exposure requires a stable phase robust to thermal and mechanical drifts. If ϕ wanders more than $\sim \lambda/4$, the net visibility γ will reduce and decrease S/N proportionally. Our data analysis can handle irregularly spaced phase steps, so only large ϕ-wandering has impact on γ. We use a commercial PZT-transducer mounted mirror to actively compensate for optical path fluctuations. The system uses a 'piggy-back' diode-laser that propagates parallel to and above the science beam through the interferometer elements and forms a fringe on a small CCD camera. Software analyzes the location of the fringe pattern and the PZT is moved to compensate. The same piezo-system is conveniently used to phase step ϕ as desired for reduction of detector or instrument systematic noise. We have implemented stabilization for the critical "piston" mirror motion and will extend the stabilization system to 3-dimensions to compensate for slow mirror tip or tilt. (Our experience shows that tip/tilt drifts are more benign than piston drifts, but do occur). The instrument will include a flux weighted exposure timer diode via a small pickoff (not shown) to determine the effective exposure center for accurate RV periodigram analyses and barycentric correction.

3.1. Radial Velocimetry Reference Standards

The introduction of the Iodine absorption-line reference cell was crucial to the current renaissance in precision radial velocity studies. The reference cell provides a stable zero-velocity narrow-line calibrant needed to precisely determine slight Doppler shifts over long time scales. Reference cells are still central to radial velocity studies today, although although some groups now use a Th-Ar emission lamp or a laser stabilized spectrograph instead. Doppler measurements are limited to bands where the standards have adequate transmission or dense and narrow spectral signatures.

EDI injection of emission-lamp flux is simplified in comparison to methods used for conventional spectroscopy (e.g, fiber-scrambling) because our angle-independent interferometer design imprints the same spectral fiducial comb upon both the stellar and lamp beams even if they are not exactly co-axial. Our interferometer also has an accessible secondary input path that mirrors the stellar flux path. Note that because EDI produces a repeatable transmission comb throughout all wavelengths, the comb can be used to extend velocimetry's useful bandpass beyond the reference standard's regular range.

We have identified several potential vapors for NIR absorption cells. Formaldehyde and acetaldeyde are promising candidates given their broad coverage of narrow lines. These and similar organics have high vapor pressures at low temperatures and have been measured by precise FTIR spectra. The atmosphere itself provides a dense comb of NIR narrow absorption lines, similar to that of an absorption cell. Using the detailed atmospheric absorption models of Roe (2002) we find that the atmospheric spectrum has adequate spectral feature density and slope for use as a velocimetry absorption cell at precision of >10 m/s. Atmospheric variations, including line sight velocity perturbations, will constrain the usable velocity precision.

3.2. Observing Plan

We plan to observe ∼135 cool stars at precision of ∼100 m/s, including about 100 M dwarfs with H<10 mag, 25 L dwarfs with 10<H<15, and 10 T dwarfs with 13<H<15. Our survey plan will follow other successful dynamic observing strategies. **M stars:** The catalogs of nearby M stars are still remarkably incomplete. Reid et al. (2004) estimate by extrapolating the luminosity function with 8 pc that 35% of stars within 20 pc are yet to be discovered, nearly all of them low luminosity M dwarfs. However, this situation is rapidly evolving as nearly all such stars are detected by 2MASS, and we can expect a thorough and complete inventory of nearby M stars in the near future from the NASA NSTARS project. There are presently catalogued ∼300 M stars within 25 pc in the NSTARS database, brighter than H=10, on which we can achieve a photon limited precision of $<100\,ms^{-1}$ in 1-4 minutes depending on stellar rotation. This is sufficient to detect the 300 ms^{-1} signature a 1 M_J planet in a 3 day orbit around a 0.3 $M_\odot$ star. **L and T Brown Dwarfs:** There are now ∼200 L and ∼50 T dwarfs known. As these are substantially fainter, and will therefore require significantly longer integration time, we will start with a relatively small sample of nearby targets.

ACKNOWLEDGMENTS

This work was performed under a CalSpace grant to the Space Sciences Lab., and under the auspices of the U.S. Department of Energy by the University of California, Lawrence Livermore National Laboratory under contract No. W-7405-Eng-48. D. Harbeck acknowledges the support of the Townes Fellowship program of the Space Sciences Lab. The planetary program and use of Triplespec is to be conducted with the support and participation of Dr. T. Herter of Cornell University.

REFERENCES

1. S. Vogt *et al.*, "HIRES: The High Resolution Echelle Spectrometer on the Keck Ten-Meter Telescope," *Proc. SPIE* **2198**, p. 362, 1994.
2. S. Vogt, "The Lick Observatory Hamilton Echelle Spectrometer," *PASP* **99**, p. 1214, 1987.
3. M. Mayor *et al.*, "Setting New Standards with HARPS," *The Messenger* **114**, p. 20, 2003.
4. J. D. Kirkpatrick, I. N. Reid, J. Liebert, R. M. Cutri, B. Nelson, C. A. Beichman, C. C. Dahn, D. G. Monet, J. E. Gizis, and M. F. Skrutskie, "Dwarfs Cooler than "M": The Definition of Spectral Type "L" Using Discoveries from the 2 Micron All-Sky Survey (2MASS)," *ApJ* **519**, pp. 802–833, July 1999.
5. D. Erskine, "An Externally Dispersed Interferometer Prototype for Sensitive Radial Velocimetry: Theory and Demonstration on Sunlight," *PASP* **115**, pp. 255–269, 2003.
6. D. Erskine, "Combined Dispersive/Interference Spectroscopy for Producing a Vector Spectrum," *US Patent* **6,351,307**, Feb. 26, 2002.
7. J. Ge, D. Erskine, and M. Rushford, "An Externally Dispersed Interferometer for Sensitive Doppler Extrasolar Planet Searches," *PASP* **114**, pp. 1016–1028, 2002.
8. D. Erskine and J. Ge, "Novel Interferometer Spectrometer for Sensitive Stellar Radial Velocimetry," in *Imaging the Universe in Three Dimensions: Astrophysics with Advanced Multi-Wavelength Imaging Devices*, W. van Breugel and J. Bland-Hawthorn, eds., *ASP* **195**, p. 501, 2000.
9. D. Erskine, J. Edelstein, M. Feuerstein, and B. Welsh, "High Resolution Broadband Spectroscopy using an Externally Dispersed Interferometer," *ApJ* **592**, pp. L103–L106, 2003.
10. D. Erskine and J. Edelstein, "Interferometric Resolution Boosting for Spectrographs," in *Ground-based Instrumentation for Astronomy, ed. A. Moorwood*, SPIE Proc. 5492, June 2004.
11. N. Douglas, "Heterodyned Holographic Spectroscopy," *PASP* **109**, p. 151, 1997.
12. S. Frandsen, N. Douglas, and H. Butcher, "An Astronomical Seismometer," *A&A* **279**, p. 310, 1993.
13. J. Harlander, R. Reynolds, and F. Roesler, "Spatial Heterodyne Spectroscopy for the Exploration of Diffuse Interstellar Emission Lines at Far-ultraviolet Wavelengths," *ApJ* **396**, p. 730, 1992.
14. M. Born and E. Wolf, "Principles of Optics," pp. 333–338, Pergammon Press, 6th ed., 1980.
15. R. S. McMillan, T. L. Moore, M. L. Perry, and P. H. Smith, "Radial Velocity Observations of the Sun at Night," *ApJ* **403**, pp. 801–809, Feb. 1993.

16. D. Erskine and J. Edelstein, "High-resolution Broadband Spectral Interferometry," in *Future EUV/UV and Visible Space Astrophysics Missions and Instrumentation, ed. J. C. Blades, O. H. Siegmund*, pp. 158–169, SPIE Proc. 4854, Feb. 2003.
17. J. C. van Eyken, J. Ge, S. Mahadevan, and C. DeWitt, "First Planet Confirmation with a Dispersed Fixed-Delay Interferometer," *ApJ* **600**, pp. L79–L82, Jan. 2004.
18. R. Hilliard and G. Shepherd, "Wide-Angle Michelson for Measuring Doppler Line Widths," *J. Opt. Soc. Am.* **56**, p. 362, 1966.
19. P. Connes, "Absolute Astronomical Accelerometry," *Astrph. & Spc. Sci.* **110**, p. 211, 1985.